

# Acoustic noise generation under plunging breaking waves\*

doi:10.5697/oc.55-4.809  
**OCEANOLOGIA**, 55 (4), 2013.  
pp. 809–836.

© Copyright by  
Polish Academy of Sciences,  
Institute of Oceanology,  
2013.

## KEYWORDS

Wave breaking  
Noise generation by breaker  
Wave energy dissipation

ZYGMUNT KLUSEK<sup>1</sup>  
ALIAKSANDR LISIMENKA<sup>2</sup>

<sup>1</sup> Institute of Oceanology,  
Polish Academy of Sciences,  
Powstańców Warszawy 55, 81–712 Sopot, Poland;  
e-mail: klusek@iopan.gda.pl

<sup>2</sup> Maritime Institute in Gdańsk,  
Długi Targ 41/42, 80–830 Gdańsk, Poland;  
e-mail: sasha@im.gda.pl

Received 15 March 2013, revised 1 August 2013, accepted 17 September 2013.

## Abstract

The paper presents results of investigations performed in a wave channel in order to determine associations between the dissipation of surface wave energy during breaking and acoustic noise emission.

The experiments were carried out in fresh water in the Large Wave Flume (GWK) at the Forschungszentrum Küste (FZK) in Hanover (Germany). Relationships between the acoustic noise energy and losses of surface wave energy were estimated over the broad acoustic frequency band from 350 to 12 500 Hz, and the characteristic temporal changes of the spectral properties of noise in the breaking process were demonstrated.

---

\* The experimental part of the work was supported by an EC grant ‘Transnational access to large-scale tests in the large wave flume (GWK) at the Forschungszentrum Küste (FZK)’ contract No. HPRI-2001-CT-00157.

The complete text of the paper is available at <http://www.iopan.gda.pl/oceanologia/>

It was found that the ratio of acoustic noise energy generated during wave breaking to the energy dissipation of single plunging breakers with heights of 1.6–2.8 m were in the  $10^{-9}$ – $10^{-8}$  range and found to be in reasonable agreement with the results of some previous experiments performed for smaller scales of breaking wave.

The study contributes to the development of a passive acoustic method for the parameterization of sea surface dynamic processes.

## 1. Introduction

In recent decades, acoustic oceanographers have shown increasing interest in the more accurate quantification of the characteristics of a number of dynamic processes at the air-sea boundary, such as wave energy dissipation, gas exchange rates and the nature of rain. It was suggested that further progress in this field could be made by implementing passive acoustic methods (Nystuen 1986, Ding & Farmer 1993, Means & Heitmeyer 2002, Makris & Wilson 2008).

Dynamic processes at the sea-atmosphere boundary, such as wave breaking, play a dominant role in the generation of ambient sea noise. This noise is produced over the whole spectrum of wave-breaking event intensities, from the smallest spills and splashes to stormy breakers. Nowadays, it is an accepted fact that the majority of noise in the ocean, especially in the mid-frequency audio range, is attributable to newly-formed acoustically active bubbles formed during wave breaking. Such newly-formed bubbles, entrained into the turbulent water body and excited by pressure fluctuations, oscillate in different modes emitting acoustic waves.

A key problem concerning atmosphere-ocean interaction is mass exchange. The results of numerous experiments and theoretical models have revealed that the gas transfer rate depends on the entrained bubble concentration. It was subsequently found that passive acoustic techniques would be useful for evaluating gas exchange between the sea and the atmosphere (e.g. Makris & Wilson 2008).

There are two types of bubble noise in the sea: noise in the frequency range above 1 kHz, which is the result of volumetric radial oscillations of individual bubbles (e.g. Medwin & Daniel 1990, Updegraff & Anderson 1991), and noise at lower frequencies, at which sounds are generated by bubble clouds oscillating as a whole entity (Loewen & Melville 1994).

Several laboratory and field experiments have demonstrated a correlation between surface wave energy dissipation and noise intensity. In recent years, much effort has been expended in determining the functional dependence between noise level and the parameters of wave breaking processes (Lamarre & Melville 1991, Hollett 1994, Deane & Stokes 1999, 2002, 2010, Means & Heitmeyer 2001, 2002, Deane 2012). For example,

Loewen & Melville (1991) showed in their wave channel experiment that the energy of noise is well correlated with the wave energy dissipated as a result of breaking and stated that a significant part of the dissipated energy was consumed in thrusting the air bubbles downwards. In another laboratory experiment, Lamarre & Melville (1991) showed that as much as 50% of the wave energy would be dissipated in pushing the air bubbles into the water body against buoyancy forces. Manasseh et al. (2006) developed a statistical method for acoustically identifying breaking wind waves and relating the sound to the energy dissipated.

In view of the observed relationship between the energy of the noise produced and the dissipated mechanical energy of a breaking wave, it was suggested that the dissipation of wind wave energy in the Ocean should be estimated by means of ambient sea noise measurements.

Field experiments performed by Means & Heitmeyer (2002) in the shore zone showed that there are distinct differences in the character of noise spectra for different types of wave breaking. On the basis of the slope of the noise spectra, this allows one to discriminate between plunging and spilling waves.

In the context of the scientific problem presented in this paper, most current research aiming to determine noise-wave energy dissipation relationships have been concerned with plungers of relatively small amplitude. On the basis of results of both laboratory and field experiments, different investigators have found that the ratio of acoustic energy generated during a breaking event to the dissipated wave energy extends over a very broad range, from  $1.6 \times 10^{-10}$  to  $10^{-6}$  (Table 1, section 5). Such a spread may be due to the different physical models implemented in the simulation of wave breaking processes. Simulations intended to mimic breaking processes at sea have sometimes been quite different from real wave breaking. Moreover, such investigations have been performed in diverse environments, i.e. in fresh or saline water or with different surfactants on the freshly formed bubble surface, which influences the spectra and concentration of the bubbles formed (Chanson et al. 2006).

As an example, in a study by Carey et al. (1993) in a fresh water lake, bubble clouds were generated by tipping a trough filled with salt water and fresh water. In experiments carried out by Kolaini & Crum (1994), the trials were conducted in an anechoic tank used as a wave making facility or in bubble plumes generated by a transient cylindrical water jet. In turn, small amplitude surface waves of the scale of a few decimetres were generated in a 3D wave laboratory experiment (Tegowski 2004). But, of all the various experiments cited above, we believe that only the investigations

by Kennedy (1992) and Ding & Farmer (1993) were conducted under more realistic conditions.

It is important to realise that it is not fully understood in what way the results of experiments performed in fresh water are comparable with those performed in saline water. In fact, rather controversial results can be found in the literature regarding the efficiency of noise generation in saline and fresh water during wave breaking simulation. Kolaini (1998) documented a 3–4 dB increase in the noise pressure level from the bubble cloud in salt water compared to the similar breaking process in fresh water. This phenomenon was attributed not only to the changes in the size spectrum of the bubbles but also to their concentrations after breaking and to changes in the thermal damping of bubbles. Moreover, bubbles entrained in a salt water environment are smaller and outnumbered in comparison to a bubble population in fresh water. This finding was supported by Cartmill & Su (1993), who stated that over a broad range of bubble radii from 34 to 1200  $\mu\text{m}$ , there was an increase in bubble density of one order of magnitude for salt water (30 PSU) versus fresh water.

In contrast to the results of Carey et al. (1993) experiments, the investigations performed by Kolaini & Crum (1994), Kolaini et al. (1994) and Kolaini (1998) demonstrated a lower spectral level of noise in fresh water than in salt water. In turn, Orris & Nicholas (2000) established that identical jets of fresh and salt water impinging perpendicularly on a water surface emit noise with different spectral-energy characteristics. The noise level from a fresh-water jet in the 300–1100 Hz frequency range was 15 dB (!) higher than in a salt-water environment. The authors warned against comparing data gathered during experiments on sound generation by turbulent water performed in saline and fresh water.

This paper presents the results of underwater noise measurements conducted under single plunging wave breaking in the Large Wave Flume (GWK) at the Forschungszentrum Küste (FZK) in Hanover (Germany). Owing to the scale of the facility, it was possible to extend earlier experiments to a larger scale in which wave heights correspond to moderate sea state conditions when the wind speed reaches values of  $15 \text{ m s}^{-1}$ . Moreover, the total energy of wave packets, which may be up to 900 kJ, is many orders of magnitude higher than in other laboratory experiments.

It can be reasonably assumed that the noise parameters measured in the vicinity of such a single plunging breaker should reflect wave breaking in shallow water. However, as in other similar experiments, the quantities characteristic of the wave breaking process in shallow water may not adequately represent conditions in the open deep sea.

The paper is organized as follows. Section 2 briefly discusses and gives examples of the energy and spectral parameters of breakers generated during the experiment. In section 3 the acoustic setup, methods and signal post-processing are reported. Section 4 presents the acoustic noise parameters during the experiment. The outcomes of these sections are combined in section 5, which gives relationships between the noise energy and surface wave energy and derives the algorithm for computing the acoustic energy generated during the breaking process on the basis of ray acoustics. Finally, the results of the experiments are discussed.

## 2. Surface wave measurements and processing

### 2.1. Wave channel

The experiments were conducted in the Large Wave Flume (GWK) at the Forschungszentrum Küste (FZK) in Hanover (Germany). The channel (overall length 307 m, depth 7 m, width 5 m) was filled with fresh water at a temperature of 6°C at the moment of the experiment (Figure 1).

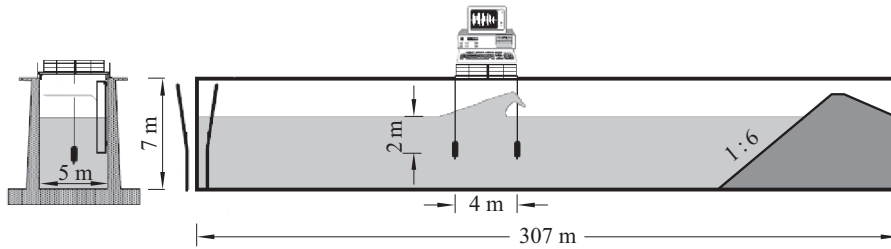


**Figure 1.** Large Wave Flume (GWK) and measurement setup

Single wave breakers were produced by a computer-operated mechanical piston-type wave maker. Due to the constructive interference of different wavelength components of a wave packet travelling with different phase velocities, single breaking events are created with the required amplitude and at the required point. Free surface elevations were recorded using the set of 12 wave gauges non-equidistantly attached to the channel wall. The geometry of the wave gauge allocation throughout the experiments is illustrated in Figure 2.

The wave gauge locations are shown as vertical lines with circles at the top. The sampling frequency of the surface elevation data was 200 Hz and 16-bit resolution for each channel with samples taken simultaneously. After low-pass filtering with  $f_{\text{cutoff}}$  equal to 2 Hz, surface elevation data were resampled with a 4:1 ratio.

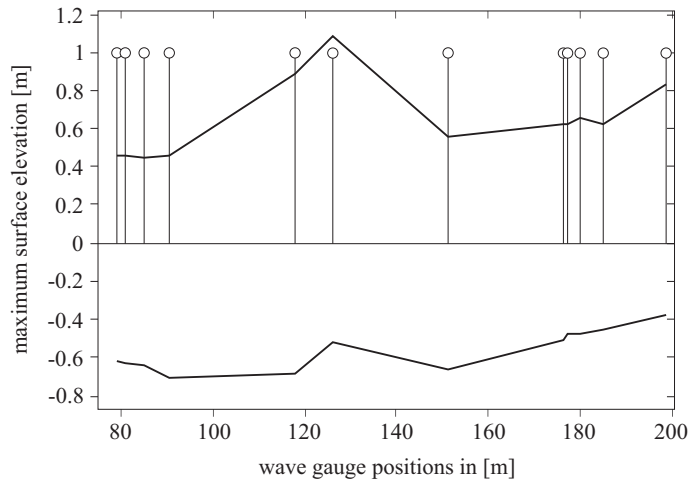


**Figure 2.** Positions of the wave gauges during the experiment and an example of the history of changes of the maximum and minimum surface elevation (relative to the undisturbed water level) registered along the channel in a wave train

This experiment was complemented with the registration of the acoustic noise at two points, positioned on both sides of the wave breaking zone. For correct interpretation of the acoustic results, visual observation and video recording of the water surface displacement were done concurrently.

## 2.2. Wave characteristics

The plunging events were generated using single wave packets with linearly decreasing frequency and increasing amplitude. A wave train was generated by a computer-controlled wave generator in such a way that the wave energy was focused at an arranged location and resulted in a plunging breaker. The breakers with a wave height above 1.6 m broke with the formation of a plunging jet at the crest and subsequent splash. In all of the runs, after plunging, the waves evolved into quasi-spilling waves, a bora-like form. However, for the highest-energy waves it was observed that the first higher splash was followed by another one.

Runs were repeated three times for each wave height with exactly the same wave generator time series. Altogether 22 runs were completed, and in three cases spilling breaker events were generated for different wave packet energies. To be sure that the noise results were entirely repeatable, each wave packet generation was followed by a period of calm lasting about 20–30 minutes, which allowed the water surface to settle and the bubbles produced earlier to dissipate. The character of the wave propagation ranged between the intermediate and deep type of gravity waves.

The maximum wave height recorded in the experiment and defined as the crest-to-trough distance before the breaking point was 2.7 m, which corresponds to open sea wave conditions with a force 4–6 wind. Examples of time series of the water surface elevation in a wave packet propagated down the channel are presented in Figure 3.

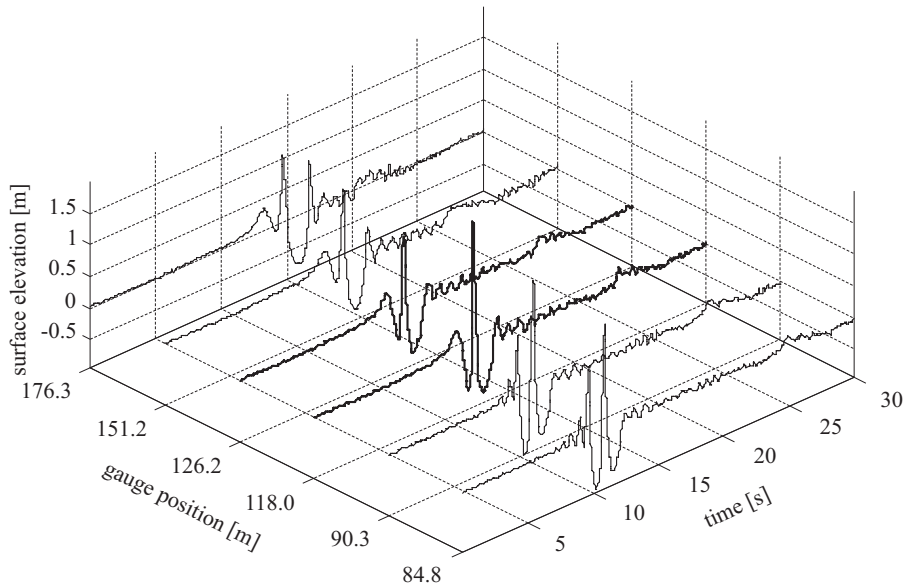


**Figure 3.** Temporal evolution of a wave packet registered along the Wave Flume at various wave gauges. The breaking area is located between the gauges positioned at 118.0 and 126.2 m (bold lines)

The surface elevation displacement data were registered at distances from the wave maker of 84.85, 90.29, 118.0, 126.22, 151.20 and 176.30 metres. Figure 3 illustrates wave packets with periods  $t$  of components ranging between 1.29 and 4.28 seconds.

The evolution of the wave packet registered at two adjoining wave gauges is presented in Figure 4. The main frequency components were easily recognized and the local phase velocity for each of them was readily determined from an estimate of the retardation time between two local maxima.

In general, the estimation of wave energy flux requires full information about the velocity and pressure fields recorded at the same time as the surface displacement. In practice, however, realistic values were obtained only if the group velocity of a wave packet and the surface displacement were known (e.g. Nepf et al. 1998, Massel 2013).

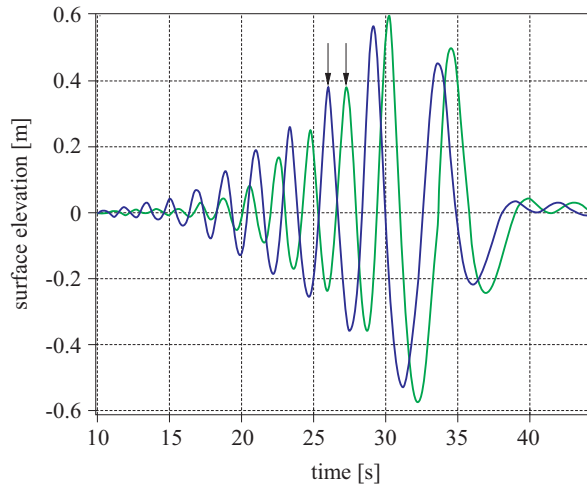


**Figure 4.** The dispersion of frequency components in a wave packet. The different frequency components are easily recognized, and the local phase velocity for each of them was readily estimated

According to the equipartition hypothesis within the framework of linear wave theory, it was assumed that the total energy of a wave packet was twice its potential energy.

As a consequence of wave velocity dispersion, the shape of the wave packets gradually changed and the group velocity was computed within two clusters of three closely-grouped wave gauges. Some difficulties cropped up in the identification of the correct time lag near the breaking zone because of substantial changes in the wave packet form between successive wave gauges. The surface displacement time series were collected from the group of three wave gauges placed ahead of the breaking point and from another three positioned down the channel reasonably far from the aerated region of the breaker.

The potential energy  $E_p$  of a wave train in the wave channel at position  $x_i$  can be expressed as follows:

$$E_p(x_i) = \frac{1}{2} \rho_w g L C_g(x_i) \int_{\tau} \zeta^2(t) dt, \quad (1)$$

where  $\rho_w$  – water density,  $g$  – acceleration due to gravity,  $C_g$  – group velocity of a wave packet,  $L$  – channel width,  $\tau$  – integration time chosen on the basis of the wave packet persistence (limited to the time during which regular surface wave phase changes were being observed),  $\zeta$  – water surface elevation recorded at the wave staff.

The group velocity is calculated from an estimate of the cross-correlation function of the surface elevation time series. Time series recorded at successive pairs of wave gauges were correlated and the time delay of the maximum cross-correlation function was used to calculate the mean group velocity of a packet  $C_g(i, i + 1)$  between two adjacent wave recorders designated  $i$  and  $i + 1$ , where  $i \in [1, N - 1]$ ,  $N = 12$ . The correlation function  $R_{ij}$  of two surface water displacement time series  $\zeta_i$  and  $\zeta_j$  registered at the wave gauges  $i$  and  $j$  is defined as

$$R_{ij}(x_i; x_j, \tau) = E \{ \zeta(x_i; t + \tau) \zeta(x_j; t) \}, \quad (2)$$

where  $E\{\cdot\}$  denotes the expectation operator.

The mean group or phase velocities are calculated between adjacent pairs of wave gauges, i.e. with positions of  $(x_i, x_{i+1})$ . Consequently, in order to estimate the group velocity at the  $i$ -th wave gauge,  $C_g(x_i, x_{i+1})$  was interpolated at the wave gauge positions.

The wave gauge positions were selected at points where the changes in wave packet shape were rather insignificant.

Representative results of cross-correlation functions obtained for a breaker are exemplified in Figure 5.

The group speeds of wave packets were found to be in the 3–6 m s<sup>-1</sup> range. The dissipation of wave packet energy was estimated on the basis of the surface elevation time series acquired from selected wave gauges. The two sets of group velocities were computed on the basis of the time series obtained at wave gauges 2, 3 and 4 placed before the breaking area (at distances 81.15, 84.85 and 90.29 m from the wave maker) and at wave gauges 8, 9 and 10 placed after the breaking point (at 176.30, 177.4 and 180.0 m). It was assumed that at the position of the second wave gauge cluster, any inaccuracy in the estimation of the surface displacement associated with the effects of gas bubbles and the further rise of the water level after breaking was moderate. The average of a minimum of 3 runs for each wave height gives a wave packet's ensemble average.

It was observed that the group velocity varied along the channel, i.e. in relation to the different wave spectral components. The group velocity of a wave train reached maximum values when it achieved its greatest height, immediately before wave breaking. Moreover, the mean wave group velocity is characteristic of transitional waves and is less than the phase wave velocity of shallow water waves, which is 7 m s<sup>-1</sup> for a mean water depth of 5 m (Massel 2013).

In turn, the wave packet energy usually reached a minimum at the wave gauge situated 126 m from the wave maker. This is due to the inaccuracy in the wave gauge readings near the breaking point because of the impact

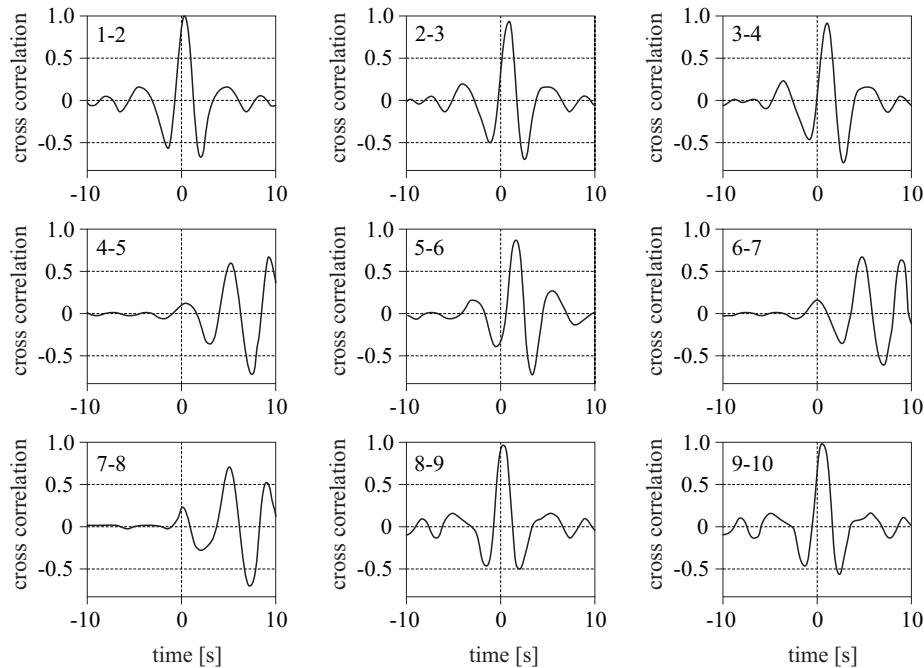


**Figure 5.** The cross-correlation functions of the surface elevation time series for different pairs of wave gauges. The wave gauge numbers are given in the upper left corners of the plots; the smaller number refers to the position closer to the wave maker, as shown in Figure 2

of air bubbles. The reduction in the wave packet energy caused by friction along the bottom and the tank walls is insignificant compared to the energy losses incurred during wave breaking. Consequently, the differences in wave energy before and after the collapse of a single wave may be regarded as the dissipation due to wave breaking only.

The dependence of the energy dissipation rate in the breaking process on different initial wave-packet energies is shown in Figure 6. It is evident that the dissipation rate in breaking waves is sensitive to the character of the wave. Owing to the different spectra of the wave packets, spilling waves were generated in the three events. Dissipation rates in the breaking waves are clearly distinguished in the figure between spilling events, shown by diamonds, and plunging breakers, indicated by squares. The dissipation rates are noticeably lower for spillers than for plunging breakers.

The absolute values of the dissipated energy for plunging wave packets lie between 22 and 320 kJ. The results are comparable with the predicted rate of energy dissipation per unit length of the wave crest (more precisely, the mean wave energy dissipation at the unit wave crest per unit

time), initially proposed by Duncan (1981) and later corrected by Melville (1994):

$$\varepsilon_L = a 10^{-3} \rho_w C_p^5 / g, \quad (3)$$

where  $a$  – coefficient estimated by Melville (1994) in the range  $a \in 3.2\text{--}16$ , with a lower value for spilling breakers and a higher one for more severe plungers, and  $C_p$  – wave phase speed.

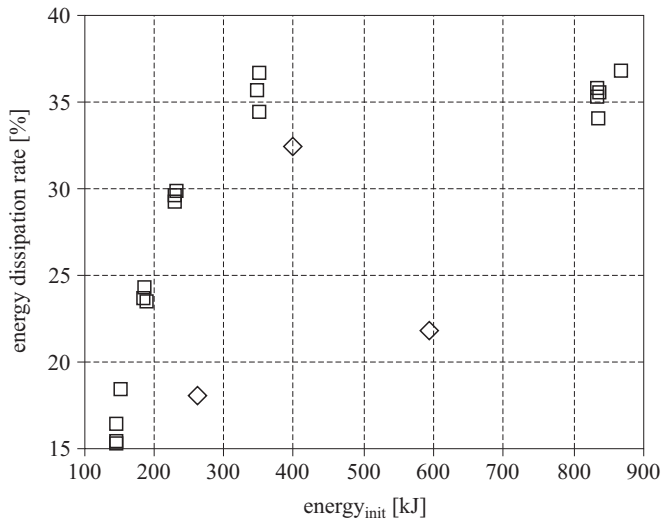


**Figure 6.** The dependence of the energy dissipation rate during wave breaking as a function of the initial wave energy in a wave packet. Spilling events are marked by diamonds ( $\diamond$ ), and plunging breakers by squares ( $\square$ )

For plungers, the predicted wave energy dissipation rate in a 5 metre wide channel is of the same order as that found in our experiments:  $63.5 \text{ kJ s}^{-1}$  for the stormiest waves (for  $a = 16$ ) and for a phase speed of the dominant component in the spectra equal to  $6 \text{ m s}^{-1}$ .

The rate of energy dissipation during plunging depends nonlinearly on the initial energy. With increasing packet energy, the dissipation rate rises from about 15% for the lower-energy waves to nearly 40% in the largest turbulent wave breaking, which is in quantitative agreement with earlier investigations (Melville 1994). However, for the most violent breakers with a wave height of ca 2.7 m, dissipation processes became saturated.

### 3. Noise measurements and processing

Acoustic noise recordings were performed using two home-made omnidirectional hydrophones placed at 2 m depth and 4 m apart horizontally along

the channel axis (Figure 1). The location of the hydrophones in the channel changed from approximately 110 to 130 m relative to the wave generator. The hydrophones were attached to a mobile observation platform positioned slightly behind the most intensive breaking area. Because the recording was conducted near the breaking point, it was rational to expect that the spectrum of the recorded noise would appropriately reproduce the spectrum of the source, i.e. acoustically active bubbles.

The acoustic signal was acquired with a 16-bit resolution Gage Analog Digital Converter with sampling rates in each of the two channels equal to 50 Ksamples  $s^{-1}$ . Sound registration was started in advance of a wave packet approaching the platform.

To prevent saturation of the preamplifier by hydrodynamic pressure from the oscillating water surface level, which is many orders of magnitude greater than the acoustic signal, the high-pass analogue filter was set at the preamplifier input. The preamplifier bandwidth was in the range from 350 Hz to 35 kHz. Additionally, a low-pass filter was installed to match the Nyquist frequency limit. The hydrophones were calibrated at low frequencies in the sea and at high frequencies in the calibration tank, using as reference the manufacturer's calibrated Brüel-Kjær type 8104 hydrophone. The results of calibration tests showed that the hydrophones had an approximately spherical directivity pattern and a flat frequency response in the broad operating frequency range.

Since collective oscillations of bubbles in a bubble plume are usually observed at frequencies below 400 Hz (Schindall & Heitmeyer 1996), the registered and analysed component of the noise should be related to sound generated by single bubbles or small air pockets, rather than to bubble clouds as a whole.

In order to estimate the duration of the noise generated by active bubbles, the background noise level of the flume was taken into account. The averaged background noise spectra were summed before and after surface wave packet propagation, and their levels were taken to be the minimum spectra level of a breaking signal.

The sound records were stored on a disk and post-processed. High-resolution power spectra were calculated using the FFT algorithm of sub-samples with a rectangular window and averaged in 1024 frequency bands. One-third octave frequency band spectra were calculated with a set of numerical filters with centre frequencies equally spaced on the logarithmic scale (350, 400, 500, . . . , 12 500 Hz).

#### 4. Characteristic features of the noise

Regardless of the different sound propagation conditions in the wave channel compared to the deep ocean and reported differences in the bubble size spectra in fresh and saline water, the obtained slopes of the noise spectrum level are only slightly different to those obtained in the sea from plunging breakers (Deane 1997, Means & Heitmeyer 2002). The broad maximum in the acoustic spectrum of the breaking event occurs between 500 and 2000 Hz, with the peak at 1 kHz, which is commonly reported for open sea observations.

Examples of the time evolution of the noise power spectral density for the period of breaking registered at both hydrophones in the selected 1/3 octave frequency bands are given in Figure 7.

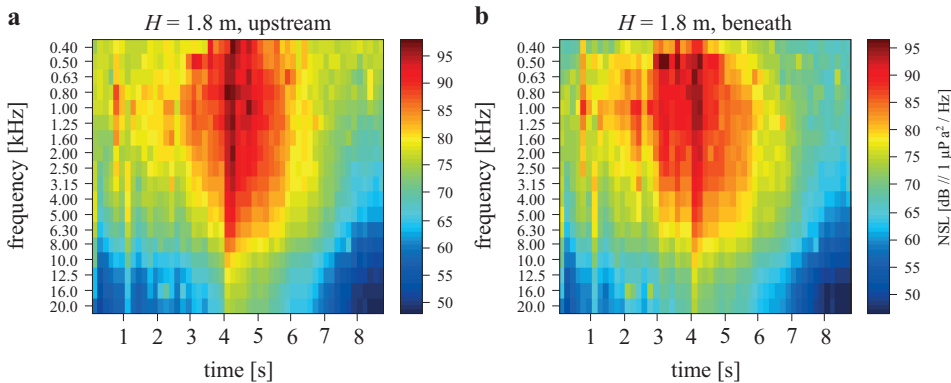


**Figure 7.** Temporal evolution of the noise spectrum level during a breaking event. Spectra are averaged in 1/3-octave frequency bands [dB re  $1 \mu\text{Pa}^2/\text{Hz}$ ]. The instantaneous spectrum measured upstream 4 m from the breaking area (a) and beneath the breaking area (b)

It was observed that at the hydrophone situated nearer to the wave generator, the noise level began to increase as the wave was approaching, before breaking occurred. It is thought that the noise preceding breaking could be produced by the turbulence of the surging water mass near the channel walls and by bubble formation processes at the wave edge. Moreover, it was observed during the experiments that the crest of an incipient plunger was bubbling slightly; this could have been responsible for the observed precursor of the signal's main fraction. A similar precursor stage of the noise was reported in the sea observations conducted by Deane (1997) for spillers and by Bass & Hay (1998) for plungers. This inclines one to reject the hypothesis that processes associated with friction along the channel sides may create a substantial fraction of the precursor noise.

The sound became significantly louder when the wave edge overturned and hit the water surface at the wave trough; the duration of this phase was about half a second. The most important differences in the noise characteristics between the two hydrophones were its intensities. The difference in noise level at the hydrophones was about 4 dB. The higher signal level was registered at the hydrophone positioned inside or, in the case of lower wave heights, under the breaking volume. Despite the high level of noise generated during wave breaking, squeaks emitted by the wave generator mechanisms and spikes associated with the jerking of the hydrophones by the turbulent wave stream were audible.

The temporal changes of noise spectral signatures during the breaking process registered at both hydrophones are illustrated in Figure 8.

The upper panel in Figure 8 shows the noise levels computed at 0.08 s intervals for the whole registered frequency band, i.e. 350–12 500 Hz. The middle panel shows the mean frequency (defined as the ratio of the 1st spectral moment to the 0th spectral moment – Massel 2013) for the same frequency range. Using the ordinary least-squares estimation method, the

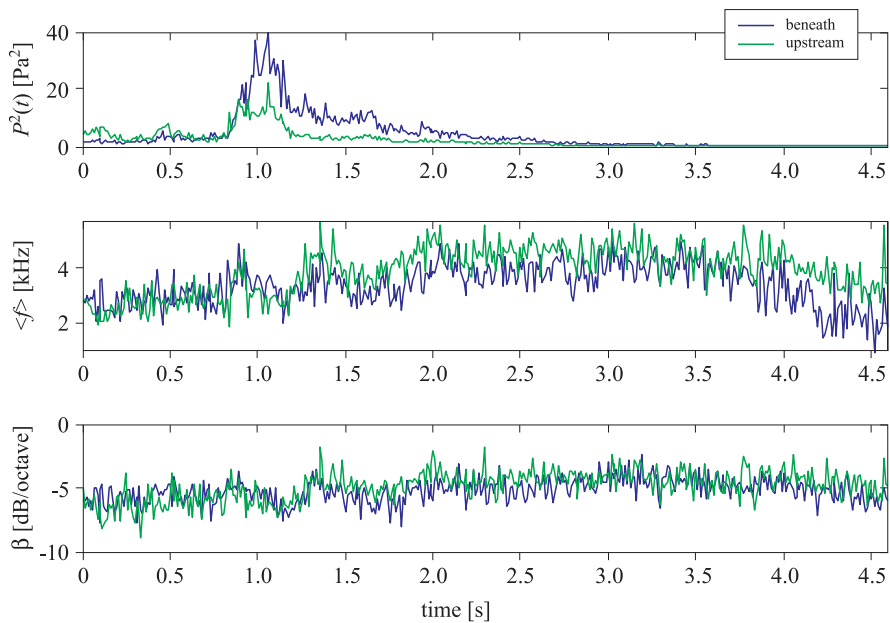


**Figure 8.** Temporal evolution of the mean-square of the acoustic pressure and selected spectral parameters of the noise (mean frequency and noise spectra slope) during wave breaking. The noise was registered beneath the bubble plume (blue curves) and 4 m upstream of the breaking area (green curves). The data are for  $H = 1.8$  m of a wave packet height

spectrum slopes [dB/octave] in the frequency range from 1500 to 12 500 Hz were calculated in the log-log scale (bottom panel). Generally, it was observed that in the first half second during rolling, the mean frequency displays shifted towards higher frequencies and were correlated with changes in the spectral slope.

A rapid rise in the pressure amplitude can be seen at the beginning of the breaking process when the wave edge impinges on the water surface, after which there is a slow decay with no beats, due mainly to the random (chaotic) nature of the noise sources. After plunging, the active sound generation phase depends on the wave intensity, which in our experiments lasted up to ca 3 s. The noise intensity decayed exponentially in time, and in the first 2–4 s after the maximum value, the noise level in the analysed frequency band had a characteristic slope:  $-7 \text{ dB s}^{-1}$  for wave heights  $H = 1.6\text{--}2.0 \text{ m}$  and  $-4.5 \text{ dB s}^{-1}$  for  $H = 2.4\text{--}2.7 \text{ m}$ .

The increase in sound intensity was faster than the decay, which is in agreement with earlier observations from seashore experiments reported by Bass & Hay (1998).

The negative slope of the spectrum above 1500 Hz was about  $-6 \text{ dB/octave}$ , momentarily reaching a minimum value up to  $-10 \text{ dB/octave}$  in the first second of breaking. In the last phase of breaking, the high-frequency portions of the sound spectra had negative slopes of from about  $-5$  to  $-6 \text{ dB/octave}$ , which were similar to the values recorded for noise spectra in the Ocean.

It was also noticed that at the plunging instant, the location of the mean frequency was shifted towards higher frequencies. This may have been due to the greater contribution of individual bubble oscillations to the whole noise field. The slope of these spectra begins at higher frequencies and is the same as that reported by Means & Heitmeyer (2002) in the surf zone. It is also the same, though at lower frequencies, as that obtained from the wave tank measurements performed by Papanicolaou & Raichlen (1988). For frequencies above 2 kHz, the slope of the spectrum was lower compared to Means & Heitmeyer's (2002) observations, where the spectral envelope for plunging waves was  $-10 \text{ dB/octave}$  and for spillers was  $-8.3 \text{ dB/octave}$ , or  $-15 \text{ dB/octave}$  as reported by Deane (1997).

It is characteristic of the mean spectra that with increasing energy in the wave packets (in our case – with increasing wave height), the maximum is relocated towards higher frequencies.

Although the registered noise spectra are reasonably similar for all wave heights, their levels do depend slightly on the position of the hydrophone(s) (Figure 9).

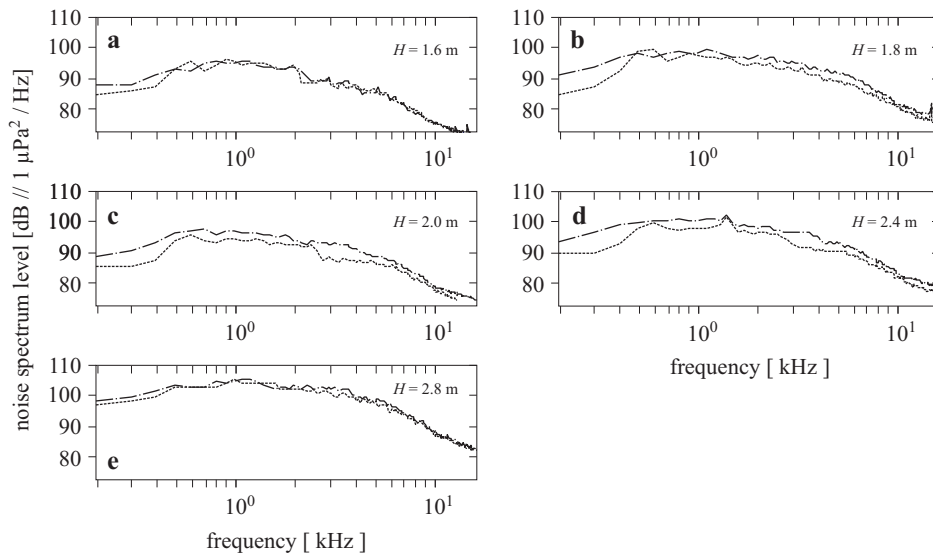


**Figure 9.** Noise spectra averaged over a single breaking event for wave heights  $H = 1.6, 1.8, 2.0, 2.4,$  and  $2.8$  m outside the breaking area (dashed line) and beneath the breaking area (dash-dot line)

The differences in noise spectra obtained here and in other laboratory experiments could also be attributed to differences in surface wave characteristics, or might be affected by the wave tank's boundary properties. It is clear that the intensity of the noise recorded in the channel at some distance from the breaking area, due to multiple reflections from the water surface, tank bottom and walls, should be higher than in an unlimited space. Similarly, some differences between our noise spectra and the noise spectra registered in the sea (Deane 1997, Bass & Hay 1998) may be due to the fact that our experiment was performed in fresh water.

Initially, it was thought that predicting the temporal evolution of the acoustic pressure and its spectra registered outside the bubble cloud on the basis of noise records within or immediately beneath the breaking volume might be problematic. Generally, it was assumed that during the most active phase of breaking, the hydrophone, which was immersed in the bubble-formation zone, registered noise from a relatively small volume surrounding the observation point. In this case, however, the acoustic properties of the wave channel walls did not influence the noise level or noise spectrum. This is because the sound absorption coefficient in a bubble cloud takes values from tens to hundreds of  $\text{dB m}^{-1}$  (Deane 1997). Hence, the noise recorded outside a bubble cloud comes only from the thin outer layer.

## 5. Noise intensity – wave energy relationships

### 5.1. Estimating the noise energy

In view of the extension of the sound generation volume in relation to the channel dimensions and the recording distance, it is inappropriate to use the model of a dipole point source placed in an unlimited medium (Kolaini & Crum 1994, Tegowski 2004) for estimating the source intensity. At the observation point outside the breaking area, multiple reflections at the channel boundaries result in an increase in the measured sound intensity. In general, the effect is predicted by the theory of sound in an enclosed space. However, in our case, the sound sources extended over a significant part of the channel's cross-section and were additionally accompanied by altered sound attenuation due to changes in bubble concentration, size spectrum and entrainment depth. It seems that there is no easy and accurate method for predicting the influence of reverberation on the observed source level.

In order to evaluate the impact of reverberations on the noise level, the reflection coefficient of the channel's sidewalls and floor was estimated on the basis of tests performed with the emission of short omnidirectional pulses. The first hydrophone was placed 0.8 m from the mechanically generated short pulse source, while the other one was situated 4 m from the source (on the horizontal axis of the channel). It was noticed that a significant fraction of the acoustic energy arrived from multiple reflections and, typically, several propagation paths between the source and the receiver were recognized. Autocovariance processing of the signal enabled the first few paths of the scattered signal to be separated. The results of the tests indicated that the pressure reflection coefficient from the channel walls, in a one-octave frequency band with 5 kHz centre frequency, in the case of angles of incidence close to vertical, varied around a value of 0.75, which is quite close to the theoretical prediction for concrete walls.

Furthermore, in order to estimate the influence of wall reflections on the registered noise level and hence on the calculation of the acoustic energy emitted by a breaker, the numerical model based on the theory of 'image' sources was implemented (Brekhovskikh & Lysanov 1982). The overall sound field registered by the hydrophone is the sum of direct contributions from noise sources (situated at the boundary of the bubble cloud) and from a series of 'image' sources produced by multiple reflections from the channel's side walls and floor, and from the water surface. The total sound field at the hydrophone can be estimated by summing up incoherently the contributions from each of these sources.

The pressure reflection coefficients at the boundaries  $\alpha$  were:

- $\alpha_{x1} = 0$  at the surface where the sources are distributed, and  $\alpha_{x2} = 0$  at the opposite wall (open channel in the upstream direction);
- $\alpha_S = 0.9$  and  $\alpha_B = 0.75$  at the water surface and the channel floor respectively;
- $\alpha_{W1} = \alpha_{W2} = 0.75$  at the channel walls.

The pressure at  $\vec{X} = [x_r, y_r, z_r]$  from an elemental source with unit amplitude positioned at point  $\vec{X}' = [x_s, y_s, z_s]$  can be schematically stated as the sum:

$$\begin{aligned}
 p(t, \vec{X}, \vec{X}') = & \frac{\delta[t - (r_0/c_w)]}{r_0} + \frac{\delta[t - (r_B/c_w)]}{r_B} \alpha_B + \\
 & + \frac{\delta[t - (r_S/c_w)]}{r_S} \alpha_S + \frac{\delta[t - (r_{W1}/c_w)]}{r_{W1}} \alpha_W + \dots \\
 & + \frac{\delta[t - (r_{W2}/c_w)]}{r_{W2}} \alpha_W + \frac{\delta[t - (r_{BS}/c_w)]}{r_{BS}} \alpha_B \alpha_S + \\
 & + \frac{\delta[t - (r_{SB}/c_w)]}{r_{SB}} \alpha_B \alpha_S + \frac{\delta[t - (r_{SW}/c_w)]}{r_{SW}} \alpha_W \alpha_S + \dots,
 \end{aligned} \tag{4}$$

where  $r$  – the length of the path from the elemental ‘image’ source to the receiver through reflections at the bottom, side walls and water surface,  $r_{BS}$  – the path between a source and the receiver reflected from the channel bottom ( $B$ ), the channel wall ( $W$ ) and the water surface ( $S$ ),  $\alpha_S$  – the Rayleigh reflection coefficient at the water surface,  $\alpha_B = \alpha_W$  between the water and the channel’s hard boundaries,  $\delta$  – the Dirac delta function.

The series was truncated when the level of  $p(t, \vec{X}, \vec{X}')$  calculated along a path was below  $-20$  dB (in relation to the pressure at unit distance). Figure 10 depicts the noise source random distribution on a semi-cylindrical surface (shaded) and gives examples of sound paths between a source and the point of observation (with designated pressure reflection coefficients).

The excess amplification due to multiple reflections, defined as the ratio of the total sound energy at the receiver location  $\vec{X}$  to the free-field sound energy at the same point from the extended source of the same size was calculated using equation (4).

For a more detailed explanation, the reader is referred to the literature (e.g. Allen & Berkley 1979, Hammad 1988). A similar method, though limited to the 2D case, was used by Deane (2000) in his analysis of the influence of the bubble curtain on noise absorption in a very shallow sea.

The estimates were obtained by making some simplifying assumptions. The propagation paths between sources located on a bubble cloud of known

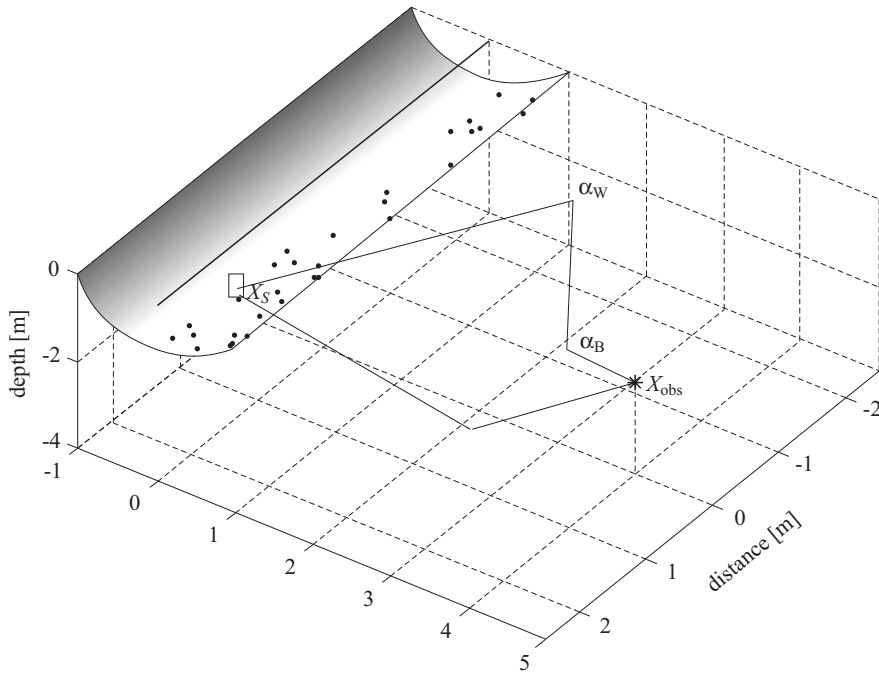


**Figure 10.** Distribution of elemental noise sources on a semi-cylindrical surface and the sound paths: examples between the source  $X_S$  and the point of noise registration  $X_{obs}$  located upstream of the breaking area

geometry and the receiver are straight lines. The type of wall material (flat, compressed concrete surfaces) meant that sound diffusion could be disregarded and that the reflection coefficient of the boundaries could be assumed independent of the angle of incidence.

It was considered that the noise field comes from a continuous distribution of random monopole sources located in the thin shell that makes up the surface of the horizontal semi-cylinder of radius equal to the bubble entrainment depth and the axis of which lies at the undisturbed water surface. Based on the above model, a set of normalized pulses which represent the pressure and time delay for paths between point sources and the receiver was generated.

However, the evaluation of the penetration depth of an acoustically active bubble cloud in sea water as well as in the channel remains ambiguous. According to Garret et al. (2000), the maximum penetrating depth of the cloud under spilling breakers in the sea is about one half of the breaking wave height. Nevertheless, in a series of experiments performed by Klusek & Jakacki (1997) in the Baltic Sea, a deeper bubble cloud entrainment, down to 10 m depth, was observed for a similar wind-wave height.

In their study carried out in a water tank, Chanson & Lee (1997) proposed an empirical dependence between breaker parameters and bubble entrainment depth. These authors gave a functional relationship between the relative wave energy dissipation, wave amplitude and bubble penetration depth. Transformation of their formula (4) enabled the bubble entrainment depth to be obtained as a function of the single trial wave packet parameters – the relative energy dissipation in the breaker and the wave height before breaking:

$$D_p = 0.5H_{\max} \left( \frac{1}{31.2} \frac{\Delta E}{E_{\text{init}}} \right)^{1/0.624}, \quad (5)$$

where  $H_{\max}$  – maximum wave height;  $D_p$  – bubble entrainment depth;  $E_{\text{init}}$  – total wave packet energy before breaking,  $\Delta E$  – wave energy dissipation.

According to formula (5), the bubble cloud entrains to depths from 0.3 to 1.8 m, and the hydrophone placed at the position of the breaking area is situated somewhat below the bubble cloud (Figure 11).

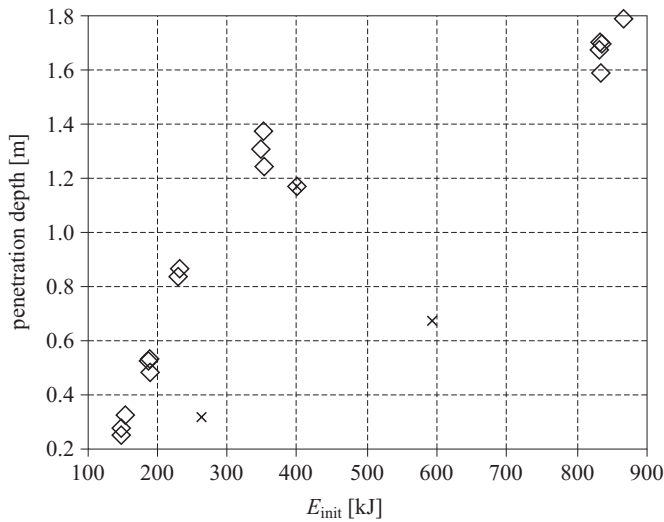


**Figure 11.** Predicted bubble penetration depth as a function of the initial wave packet energy, according to the formula given by Chanson & Lee (1997). The symbols (×) and (◇) refer to spilling and plunging waves respectively

Determining the evolution of the bubble cloud and the entrainment depth  $D_p$  of acoustically active bubbles during breaking is a complex and still insufficiently understood problem. Newly formed bubbles are pushed to the leading edge of the breaker as it propagates down the channel and are later transported deeper by turbulent motion. It is believed that

the noise is generated at the leading edge of the bubble cloud (Kolaini & Crum 1994, Andrew et al. 2001). So the bubbles located within and on the upstream boundary of the cloud contribute less to the resulting noise field at long distances as a result of rapid attenuation and scattering in the bubbling medium. As a result, the noise level is expected to be lower in the upstream part of the channel space compared to that recorded ahead of the propagating surface wave. Additionally, the noise level under the breaker, predicted from the model (eq. (4)), should be lower than that at points of observation lying some distance from the event. The reason for this may be simply explained: the sound at the point of breaking comes from the smaller surface. This was observed in all the experiments except that of the most violent breaker (Figure 12).

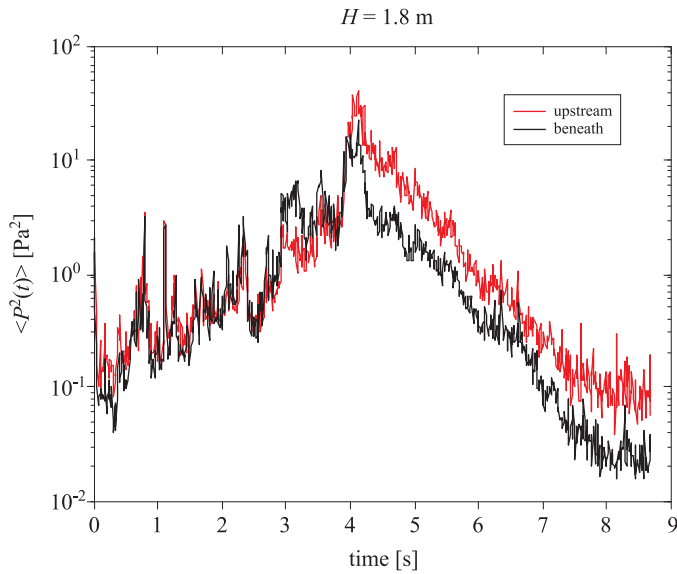


**Figure 12.** Comparison of temporal changes in the sound pressure recorded at two points – beneath the breaker (black) and at a position 4 metres upstream (red)

The noise from the sources distributed on the shoreward side of the bubble cloud can propagate only into acoustically transparent water and cannot pass upstream through it. Since the channel's walls and bottom are flat, it is not expected that sound generated at the leading edge of the plume is scattered backwards. So, upstream of the breaking area, the noise is registered solely from the sources placed to the rear and at the bottom of the plume.

The mean intensity of the noise  $\Pi$  [ $\text{J s}^{-1} \text{ m}^{-2}$ ] registered by the hydrophone over the breaking action is obtained by integrating the acoustic square pressure (Medwin & Clay 1998):

$$\Pi = \frac{1}{\rho_w c_w} \frac{1}{T} \int_0^T P_{\text{ac}}^2(t) dt, \quad (6)$$

where  $\rho_w$  – water density,  $c_w$  – speed of sound in water,  $T$  – duration of breaking event,  $P_{\text{ac}}$  – acoustic pressure.

The wave-breaking noise level was obtained after subtracting the multiple scattering from the recorded noise intensity. From the numerical model it follows that at the distances applied in the experiments, an approximately even distribution of intensity over the whole channel cross-section can be assumed. Therefore, by measuring the mean square of the acoustic pressure at a fixed point in the flume, determination of the total radiated energy flux leaving the breaking area is feasible.

It was estimated that at the point of observation with coordinates  $X_{\text{obs}}$  [4, 2.5, -2] m, in case of a roller of radius 1.0 m (with the axis on the water surface perpendicular to the long axis of the flume cross-section) and the sources distributed on the semi-cylindrical surface (Figure 10), the computed sound pressure in the semi-closed channel increased nearly four times compared to a boundless medium or in the case of complete absorption by the walls.

In general, there is qualitative agreement between the model and the results of the reverberation test experiments conducted with the short pulse source.

When computing the intensity of a noise source, an additional source of error in the calculation could be the spatial offset between the hydrophone site and the location of the noise area. These errors are not easy to quantify owing to wave progression and transformation of the breaking volume.

The estimated acoustic energy generated from a breaker bubble plume as a function of the dissipated energy of the surface wave packet for different breaking intensities is presented in Figure 13.

The results show that the rate of acoustic to wave energy ranges from  $0.1 \times 10^{-8}$  to  $0.9 \times 10^{-8}$ , depending upon the severity of the breaker. The efficiency of noise generation observed in our experiment is in the range comparable to this kind of experiments (Table 1). Only in the experiments performed by Ding & Farmer (1993) in the sea was the acoustic power radiated by breaking waves  $1.6 \times 10^{-10}$  of the rate of dissipated energy, that is, less than the observed values.

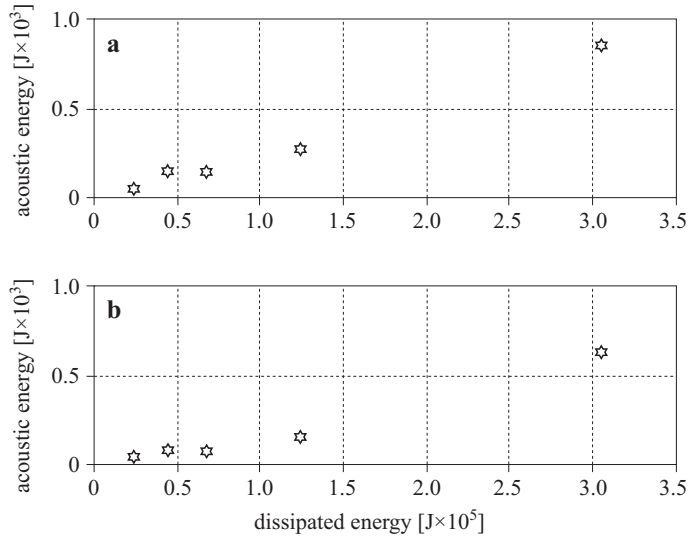


**Figure 13.** Dependence of the radiated acoustic energy on wave-packet energy dissipation. Upper panel – near breaker, lower panel – 4 m upstream

**Table 1.** Ratio of acoustic noise energy to wave energy dissipated in the breaking/plunging events presented by different authors

Authors	Type of experiment	Ratio of acoustic energy to the energy dissipated in a breaking wave event	Ratio of acoustic to wave energy
Ding & Farmer (1983, revised 1984)	deep ocean	$1.6 \times 10^{-10}$ $0.6 \times 10^{-8}$ – $4.0 \times 10^{-8}$	
Lamarre & Melville (1991)	laboratory	$10^{-8}$	
Kennedy (1992)	ocean	$10^{-6}$ – $10^{-8}$	
Carey et al. (1993)*	lake		$0.3 \times 10^{-8}$ – $2.3 \times 10^{-8}$
Kolaini & Crum (1994)	tank		$0.8 \times 10^{-7}$ – $1.09 \times 10^{-6}$ (depending on the wave energy)
Tęgowski (2004)**	shallow tank	$1.0 \times 10^{-7}$ – $4.1 \times 10^{-7}$	
this experiment	wave flume – high wave heights	$0.1 \times 10^{-8}$ to $0.9 \times 10^{-8}$ (depending on the wave energy)	

\*Ratio of the acoustic energy to the potential energy of a breaking event produced by tipping. \*\*Ratio of the mean acoustic energy to the energy dissipated in a breaking wave.

Some investigators have stated that the most active noise sources are distributed at the leading edge of the overturning wave (Deane 1997, Andrew et al. 2001). So there is a considerable probability that the noise is transmitted preferably forwards, towards still and bubble-free water, and that the sound level in front of a breaker is not comparable with that on the opposite side of the plume.

## 6. Summary

This research effort focused on investigating the dependence of acoustic noise energy on the dissipation of a single plunging wave's energy. The wave packets generated were of far higher energy than those obtained in typical laboratory experiments combining wave breaking and the accompanying acoustic noise.

The experiment was conducted in laboratory conditions with the wave packet energy ranging from 100 to 900 kJ. The results show that the rate of acoustic to wave energy is from  $0.1 \times 10^{-8}$  to  $0.9 \times 10^{-8}$ , depending upon the intensity of the breaking event.

The importance of these studies is that for the first time the acoustic energy produced by a very high energy breaking wave was measured and compared with other experiments. The findings of the present work are different from earlier studies, which explored lower-energy breaking events. It is believed that the large scale of the waves used in the experiments could also have caused this difference.

In our opinion, the result appears to offer a partial explanation at least of the saturation of the functional quadratic dependence between noise and wind speed/wave height in the sea under strong wind conditions. Farmer & Vagle (1989) explained this as being the effect of increasing attenuation of the noise propagated in the waveguide caused by the near-surface bubble layer.

Although the general picture of the relationships between noise and wave characteristics seems to be established, data on noise registration with hydrophones arranged in another configuration need to be gathered with different surface wave spectra. Due to the fact that one of the hydrophones was situated behind the overturning wave, only the noise emitted upstream of the channel (or downward of the bubbles) was registered. This part of the emitted acoustic energy probably constitutes the smaller part of the entire radiated acoustic energy, and experiments performed with hydrophones placed on either side of the breaking area could well provide more reliable results

The spectral source level density of the noise generated under the plunging breaking wave presented here should be considered solely as

an estimate; on the other hand, however, it may be very useful for estimating ambient noise levels due to breakers in the surf zone. For incipiently or calmly breaking waves typical of wind-wave conditions in a moderate ocean environment, the situation could be quite different. The characteristic patterns in the spectral parameters of the registered noise appear to be comparable to Ocean data.

In comparison to the data obtained by Ding & Farmer (1993), the lower ratios of acoustic noise energy to surface wave energy dissipation during breaking observed here could be explained as the result of the consistently smaller number of acoustically active gas bubbles produced in fresh water than in saline water.

### Acknowledgements

The authors would like to express their profound gratitude to Prof. Stanisław Massel for his support for this study.

### References

- Allen J. B., Berkley D. A., 1979, *Image method for efficiently simulating small room acoustics*, J. Acoust. Soc. Am., 65 (4), 943–950, <http://dx.doi.org/10.1121/1.382599>.
- Andrew R. K., Farmer D. M., Kirilin R. L., 2001, *Broadband parametric imaging of breaking ocean waves*, J. Acoust. Soc. Am., 110 (1), 150–162, <http://dx.doi.org/10.1121/1.1377870>.
- Bass S. J., Hay A. E., 1998, *Ambient noise in the natural surf zone: wave breaking frequencies*, IEEE OCEANS '98 Conf. Proc., 1373–1377.
- Brekhovskikh L., Lysanov Yu., 1982, *Fundamentals of ocean acoustics*, Springer-Verlag, New York, 279 pp., <http://dx.doi.org/10.1007/978-3-662-02342-6>.
- Carey W. M., Fitzgerald J. M., Monahan E. C., Wang Q., 1993, *Measurement of the sound produced by a tipping trough with fresh and salt water*, J. Acoust. Soc. Am., 93 (6), 3178–3192, <http://dx.doi.org/10.1121/1.405702>.
- Cartmill J. W., Su M. Y., 1993, *Bubble size distribution under saltwater and freshwater breaking waves*, Dynam. Atmos. Oceans, 20 (1–2), 25–31, [http://dx.doi.org/10.1016/0377-0265\(93\)90046-A](http://dx.doi.org/10.1016/0377-0265(93)90046-A).
- Chanson H., Lee J.-F., 1997, *Plunging jet characteristics of plunging breakers*, Coast. Eng., 31 (1–4), 125–141, [http://dx.doi.org/10.1016/S0378-3839\(96\)00056-7](http://dx.doi.org/10.1016/S0378-3839(96)00056-7).
- Chanson H., Aoki S., Hoque A., 2006, *Bubble entrainment and dispersion in plunging jet flows: Freshwater versus seawater*, J. Coastal Res., 22 (3), 664–677, <http://dx.doi.org/10.2112/03-0112.1>.
- Deane G. B., 1997, *Sound generation and air entrainment by breaking waves in the surf zone*, J. Acoust. Soc. Am., 102 (5), 2671–2689, <http://dx.doi.org/10.1121/1.420321>.

- Deane G. B., 2000, *A model for horizontal directionality of breaking wave noise in the surf zone*, J. Acoust. Soc. Am., 107 (1), 177–192, <http://dx.doi.org/10.1121/1.428299>.
- Deane G. B., 2012, *Surface tension effects in breaking wave noise*, J. Acoust. Soc. Am., 132 (2), 700–708, <http://dx.doi.org/10.1121/1.4730887>.
- Deane G. B., Stokes M. D., 1999, *Air entrainment and bubble size distribution in the surf zone*, J. Phys. Oceanogr., 29, 1393–1403, [http://dx.doi.org/10.1175/1520-0485\(1999\)029<1393:AEPABS>2.0.CO;2](http://dx.doi.org/10.1175/1520-0485(1999)029<1393:AEPABS>2.0.CO;2).
- Deane G. B., Stokes M. D., 2002, *Scale dependence of bubble creation mechanisms in breaking waves*, Nature, 418, 839–844, <http://dx.doi.org/10.1038/nature00967>.
- Deane G. B., Stokes M. D., 2010, *Model calculations of the underwater noise of breaking waves and comparison with experiment*, J. Acoust. Soc. Am., 127 (6), 3394–3410, <http://dx.doi.org/10.1121/1.3419774>.
- Ding L., Farmer D., 1993 *Passive acoustical measurements of scale, probability, and intensity of wave breaking*, OCEANS '93 – Engineering in harmony with ocean, IEEE Proc., Vol. 2, II-193-197.
- Ding L., Farmer D., 1994, *Observations of breaking surface wave statistics*, J. Phys. Oceanogr., 24, 1368–1387, [http://dx.doi.org/10.1175/1520-0485\(1994\)024<1368:OBSWS>2.0.CO;2](http://dx.doi.org/10.1175/1520-0485(1994)024<1368:OBSWS>2.0.CO;2).
- Duncan J. H., 1981, *An investigation of breaking waves produced by a towed hydrofoil*, Philos. T. Roy. Soc. A, 317, 331–348.
- Farmer D. M., Vagle S., 1989, *Waveguide propagation of ambient sound in the ocean-surface bubble layer*, J. Acoust. Soc. Am., 86 (5), 1897–1908, <http://dx.doi.org/10.1121/1.398568>.
- Garrett G., Li M., Farmer D., 2000, *The connection between bubble size spectra and energy dissipation rates in the upper ocean*, J. Phys. Oceanogr., 30, 2163–2171, [http://dx.doi.org/10.1175/1520-0485\(2000\)030<2163:TCBSS>2.0.CO;2](http://dx.doi.org/10.1175/1520-0485(2000)030<2163:TCBSS>2.0.CO;2).
- Hammad R. N. S., 1988, *Simulation of noise distribution in rectangular rooms by means of computer modeling techniques*, Appl. Acoust., 24, 211–228, [http://dx.doi.org/10.1016/0003-682X\(88\)90026-6](http://dx.doi.org/10.1016/0003-682X(88)90026-6).
- Hollett R. D., 1994, *Observations of underwater sound at frequencies below 1500 Hz from breaking waves at sea*, J. Acoust. Soc. Am., 95, 165–170, <http://dx.doi.org/10.1121/1.408374>.
- Kennedy R. M., 1992, *Sea surface sound dipole source dependence on wave-breaking variables*, J. Acoust. Soc. Am., 91 (4), 1974–1982, <http://dx.doi.org/10.1121/1.403681>.
- Klusek Z., Jakacki J., 1997, *On the concentrations of gas bubbles measured acoustically in the Baltic Sea – wind and time dependences*, Proc. Int. Symp. Hydroacoust. Ultrasonics, EAA Symposium (formerly 13th FASE Symposium), Jurata, May 1997, A. Stepnowski & E. Kozaczka (eds.), 103–108.

- Kolaini A. R., Crum L. A., 1994, *Observations of underwater sound from laboratory breaking waves and the implications concerning ambient noise in the ocean*, J. Acoust. Soc. Am., 96 (3), 1755–1765, <http://dx.doi.org/10.1121/1.410254>.
- Kolaini R., Roy A., Gardner D. L., 1994, *Low-frequency acoustic emissions in fresh and salt water*, J. Acoust. Soc. Am., 96 (3), 1966–1772, <http://dx.doi.org/10.1121/1.411323>.
- Kolaini A. R., 1998, *Sound radiation by various types of laboratory breaking waves in fresh and salt water*, J. Acoust. Soc. Am., 103 (1), 300–308, <http://dx.doi.org/10.1121/1.421115>.
- Lamarre E., Melville W. K., 1991, *Air entrainment and dissipation in breaking waves*, Nature, 351, 469–472, <http://dx.doi.org/10.1038/351469a0>.
- Loewen M. R., Melville W. K., 1991, *Microwave backscatter and acoustic radiation from breaking waves*, J. Fluid Mech., 224, 601–623, <http://dx.doi.org/10.1017/S0022112091001891>.
- Loewen M. R., Melville W. K., 1994, *An experimental investigation of the collective oscillations of bubble plumes entrained by breaking waves*, J. Acoust. Soc. Am., 95, 1329–1343, <http://dx.doi.org/10.1121/1.408573>.
- Makris N. C., Wilson J. D., 2008, *Quantifying hurricane destructive power, wind speed, and air-sea material exchange with natural undersea sound*, Geophys. Res. Lett., 35 (10), L10603, <http://dx.doi.org/10.1029/2008GL033200>.
- Manasseh R., Babanin A. V., Forbes C., Rickards K., Bobevski I., Ooi A., 2006, *Passive acoustic determination of wave-breaking events and their severity across the spectrum*, J. Atmos. Oceanic Technol., 23, 599–618, <http://dx.doi.org/10.1175/JTECH1853.1>.
- Massel S., 2013, *Ocean surface waves: their physics and prediction*, 2nd edn., World Sci., London–Singapore–New Jersey, 491 pp., [http://dx.doi.org/10.1142/9789814460125\\_0012](http://dx.doi.org/10.1142/9789814460125_0012).
- Means S. L., Heitmeyer R. M., 2001, *Low-frequency sound generation by an individual open-ocean breaking wave*, J. Acoust. Soc. Am., 110 (2), 761–767, <http://dx.doi.org/10.1121/1.1379729>.
- Means S. L., Heitmeyer R. M., 2002, *Surf-generated noise signatures: A comparison of plunging and spilling breakers*, J. Acoust. Soc. Am., 112 (2), 481–489, <http://dx.doi.org/10.1121/1.1491256>.
- Medwin H., Clay C. S., 1998, *Fundamentals of acoustical oceanography*, Acad. Press, San Diego, 712 pp.
- Medwin H., Daniel A. C., 1990, *Acoustical measurements of bubble production by spilling breakers*, J. Acoust. Soc. Am., 88 (1), 408–412, <http://dx.doi.org/10.1121/1.399917>.
- Melville W. K., 1994, *Energy dissipation by breaking waves*, J. Phys. Oceanogr., 24 (10), 2041–2049, [http://dx.doi.org/10.1175/1520-0485\(1994\)024<2041:EEDBBW>2.0.CO;2](http://dx.doi.org/10.1175/1520-0485(1994)024<2041:EEDBBW>2.0.CO;2).
- Nepf H. M., Wu C. H., Chan E. S., 1998, *A comparison of two- and three-dimensional wave breaking*, J. Phys. Oceanogr., 28 (7), 1496–1510, [http://dx.doi.org/10.1175/1520-0485\(1998\)028<1496:ACOTAT>2.0.CO;2](http://dx.doi.org/10.1175/1520-0485(1998)028<1496:ACOTAT>2.0.CO;2).

- Nystuen J. A., 1986, *Rainfall measurements using underwater ambient noise*, J. Acoust. Soc. Am., 79 (4), 972–982, <http://dx.doi.org/10.1121/1.393695>.
- Orris G. J., Nicholas M., 2000, *Collective oscillations of fresh and salt water bubble plumes*, J. Acoust. Soc. Am., 107 (2), 771–787, <http://dx.doi.org/10.1121/1.428253>.
- Papanicolaou P., Raichlen F., 1988, *Wave and bubble characteristics in the surf zone*, [in:] *Sea surface sound: Natural mechanisms of surface generated noise in the ocean*, R. B. Kerman (ed.), Kluwer Publ., Dordrecht, 97–109, [http://dx.doi.org/10.1007/978-94-009-3017-9\\_8](http://dx.doi.org/10.1007/978-94-009-3017-9_8).
- Schindall J. A., Heitmeyer R. M., 1996, *Breaking wave noise measurements at frequencies below 400 Hz*, J. Acoust. Soc. Am., 100 (4), 2732–2739, <http://dx.doi.org/10.1121/1.416813>.
- Tęgowski J., 2004, *A laboratory study of breaking waves*, Oceanologia, 46 (3), 365–382.
- Updegraff G. E., Anderson V. C., 1991, *Bubble noise and wavelet spills recorded 1 m below the ocean surface*, J. Acoust. Soc. Am., 89 (5), 2264–2279, <http://dx.doi.org/10.1121/1.400917>.